HERMETIC PACKAGES AND FEEDTHROUGHS FOR NEURAL PROSTHESES

Quarterly Progress Report # 5

(Contract NIH-NINCDS-N01-NS-4-2319)

(Contractor: The Regents of the University of Michigan)

For the Period:

October-December 1995

Submitted to the

Neural Prosthesis Program
National Institute of Neurological Disorders and Stroke
National Institutes of Health

By the

Center For Integrated Sensors and Circuits
Department of Electrical Engineering and Computer Science
University of Michigan
Ann Arbor, Michigan 48109-2122

Program Personnel:

UNIVERSITY OF MICHIGAN
Professor Khalil Najafi: Principal Investigator
Graduate Student Research Assistants:
Mr. Anthony Coghlan: RF Telemetry & Microstimulator Assembly
Mr. Mehmet Dokmeci: Packaging and Accelerated Testing
Mr. Mark Nardin: Microstimulator Circuit Design/Fabrication
Mr. Jeffrey Von Arx: Electrode and Package Fabrication/Testing

VANDERBILT UNIVERSITY
Professor David L. Zealear, Principal Inves:

January 1996

This QPR is being sent to you before it has been reviewed by the staff of the Neural Prosthesis Program

SUMMARY

During the past quarter we continued testing of glass packages under accelerated conditions, performed more detailed testing of the single-channel microstimulator in preparation for their manufacture and delivery to outside users, and completed the testing of the multichannel microstimulator and further characterized its on-chip transmitter and coil.

Our most significant package testing results to date are those obtained from a series of silicon-glass packages that have been soaking in DI water at 85°C and 95°C for the past year. We had one package that was soaking at 95°C. This package finally failed in this past quarter, lasting for a total of 484 days; the failure was due to the complete dissolution of the silicon substrate. We still have four of the packages that are soaking at 85°C and these have lasted now for 506 days, and are still going. The worst-case average lifetime of the packages soaking at 95°C was 119 days and that for those packages soaking at 85°C is now 257 days,. Calculation of MTTF for these glass packages using the data obtained so far indicates a worst-case lifetime of about 58 years, and a best-case lifetime of about 485 years at body temperatures.

In addition to these tests in DI water, we also started soaking the new ultrasonically-machined glass capsules in saline at the above two temperatures. These new glass capsules were bonded to thick silicon substrates. There have been a number of packages that have been soaking at 85°C, and these have provided an average lifetime of about 84 days. Packages that were soaked at 95°C all failed at various points in time, exclusively due to corrosion and dissolution of the polysilicon bonding layer in saline. This dissolution is very severe at 95°C because of the much accelerated corrosion and dissolution of silicon in saline at these temperatures. Nonetheless, we have calculated an average lifetime of about 38 days for these preliminary soaks at 95°C. Using these values, one can calculate an MTTF of about 23 years at 37°C. It is too early to draw any conclusions from the tests performed on the new packages. However, our tests so far clearly indicate that these packages can also provide an effective barrier against moisture penetration.

We also have had 5 packages soaking at room temperature in saline. One of these packages failed this past quarter, and we still have four of these under test. The longest lasting package has been soaking for 393 days at room temperature. We will continue to observe these packages for any sign of leakage.

During the past quarter we also started detailed characterization of the telemetry link for the single-channel microstiumulator. This was done because we had observed that the microstimulator did not operate correctly when used with larger transmitter coils. Our tests so far have shown that when the microstimulator receiver is within about 1-2cm of the coil windings it operates as designed; when it is centered in the middle of a 9cm diameter coil, it cannot deliver the desired pulse amplitude. This is determined to be due to the large power requirement and the limited power delivery capability of the transmitter, especially when a small 1.1mm diameter receiver coil is used. We are conducting additional tests to determine the operating range of these microstimulators.

Finally, during the last quarter we completed the testing of the bi-directional telemetry link of the multi-channel microstimulator. This device incorporates an on-chip transmitter and coil for transmitting telemetry data to the outside world, without the need for any hybrid components. We have demonstrated that data can be transmitted using a carrier frequency of about 30MHz through an on-chip coil, and can be received externally even when the external class-E transmitter is on and running. We believe this on-chip transmitter and coil can be used for many applications requiring improved reliability, in-situ monitoring of the package, or the ability to send local sensor data to the outside world. We hope to be able to provide these multichannel devices to outside users before the end of 1996.

1. INTRODUCTION

This project deals with the development of hermetic, biocompatible micropackages and feedthroughs for use in a variety of implantable neural prostheses for sensory and motor handicapped individuals. The project also aims at continuing work on the development of a telemetrically powered and controlled neuromuscular microstimulator for functional electrical stimulation. The primary objectives of the project are: 1) the development and characterization of hermetic packages for miniature, silicon-based, implantable three-dimensional structures designed to interface with the nervous system for periods of up to 40 years; 2) the development of techniques for providing multiple sealed feedthroughs for the hermetic package; 3) the development of custom-designed packages and systems used in chronic stimulation or recording in the central or peripheral nervous systems in collaboration and cooperation with groups actively involved in developing such systems; and 4) establishing the functionality and biocompatibility of these custom-designed packages in *in-vivo* applications. Although the project is focused on the development of the packages and feedthroughs, it also aims at the development of inductively powered systems that can be used in many implantable recording/stimulation devices in general, and of multichannel microstimulators for functional neuromuscular stimulation in particular.

Our group here at the Center for Integrated Sensors and Circuits at the University of Michigan has been involved in the development of silicon-based multichannel recording and stimulating microprobes for use in the central and peripheral nervous systems. More specifically, during the past two contract periods dealing with the development of a single-channel inductively powered microstimulator, our research and development program has made considerable progress in a number of areas related to the above goals. A hermetic packaging technique based on electrostatic bonding of a custom-made glass capsule and a supporting silicon substrate has been developed and has been shown to be hermetic for a period of at least a few years in salt water environments. This technique allows the transfer of multiple interconnect leads between electronic circuitry and hybrid components located in the sealed interior of the capsule and electrodes located outside of the capsule. The glass capsule can be fabricated using a variety of materials and can be made to have arbitrary dimensions as small as 1.8mm in diameter. A multiple sealed feedthrough technology has been developed that allows the transfer of electrical signals through polysilicon conductor lines located on a silicon support substrate. Many feedthroughs can be fabricated in a small area. The packaging and feedthrough techniques utilize biocompatible materials and can be integrated with a variety of micromachined silicon structures.

The general requirements of the hermetic packages and feedthroughs to be developed under this project are summarized in Table 1. Under this project we will concentrate our efforts to satisfy these requirements and to achieve the goals outlined above. There are a variety of neural prostheses used in different applications, each having different requirements for the package, the feedthroughs, and the particular system application. The overall goal of the program is to develop a miniature hermetic package that can seal a variety of electronic components such as capacitors and coils, and integrated circuits and sensors (in particular electrodes) used in neural prostheses. Although the applications are different, it is possible to identify a number of common requirements in all of these applications in addition to those requirements listed in Table 1. The packaging and feedthrough technology should be capable of:

1- protecting non-planar electronic components such as capacitors and coils, which typically have large dimensions of about a few millimeters, without damaging them;
2- protecting circuit chips that are either integrated monolithically or attached in a hybrid fashion with the substrate that supports the sensors used in the implant;
3- interfacing with structures that contain either thin-film silicon microelectrodes or conventional microelectrodes that are attached to the structure;

Table 1: General Requirements for Miniature Hermetic Packages and Feedthroughs for Neural Prostheses Applications

Package Lifetime:
≥ 40 Years in Biological Environments @ 37°C

Packaging Temperature:
≤360°C

Package Volume:
10-100 cubic millimeters

Package Material:
Biocompatible
Transparent to Light
Transparent to RF Signals

Package Technology:
Batch Manufactureable

Package Testability:
Capable of Remote Monitoring
In-Situ Sensors (Humidity & Others)

Feedthroughs:
At Least 12 with ≤125μm Pitch
Compatible with Integrated or Hybrid Microelectrodes
Sealed Against Leakage

Testing Protocols:
In-Vitro Under Accelerated Conditions
In-Vivo in Chronic Recording/Stimulation Applications

We have identified two general categories of packages that need to be developed for implantable neural prostheses. The first deals with those systems that contain large components like capacitors, coils, and perhaps hybrid integrated circuit chips. The second deals with those systems that contain only integrated circuit chips that are either integrated in the substrate or are attached in a hybrid fashion to the system.

Figure 1 shows our general proposed approach for the package required in the first category. This figure shows top and cross-sectional views of our proposed approach here. The package is a glass capsule that is electrostatically sealed to a support silicon substrate. Inside the glass capsule are housed all of the necessary components for the system. The electronic circuitry needed for any analog or digital circuit functions is either fabricated on a separate circuit chip that is hybrid mounted on the silicon substrate and electrically connected to the silicon substrate, or integrated monolithically in the support silicon substrate itself. The attachment of the hybrid IC chip to the silicon substrate can be performed using a number of different technologies such as simple wire bonding between pads located on each substrate, or using more sophisticated techniques such as flip-chip solder reflow or tab bonding. The larger capacitor or microcoil components are mounted on either the substrate or the IC chip using appropriate epoxies or solders. This completes the assembly of the electronic components of the system and it should be possible to test the system electronically at this point before the package is completed. After testing, the system is packaged by placing the glass capsule over the entire system and bonding it to the silicon substrate using an electrostatic sealing process. The cavity inside the glass package is now hermetically sealed against the outside environment. Feedthroughs to the outside world are provided using the grid-feedthrough technique discussed in previous reports. These feedthroughs transfer the electrical signals between the electronics inside the package and various elements outside of the package. If the package has to interface with conventional microelectrodes, these microelectrodes can be attached to bonding pads located outside of the package; the bond junctions will have to be protected from the external environment using various polymeric encapsulants. If the package has to interface with on-chip electrodes, it can do so by integrating the electrode on the silicon support substrate. Interconnection is simply achieved using on-chip polysilicon conductors that make the feedthroughs themselves. If the package has to interface with remotely located recording or stimulating electrodes that are attached to the package using a silicon ribbon cable, it can do so by integrating the cable and the electrodes again with the silicon support substrate that houses the package and the electronic components within it.

Figure 2 shows our proposed approach to package development for the second category of applications. In these applications, there are no large components such as capacitors and coils. The only component that needs to be hermetically protected is the electronic circuitry. This circuitry is either monolithically fabricated in the silicon substrate that supports the electrodes (similar to the active multichannel probes being developed by the Michigan group), or is hybrid attached to the silicon substrate that supports the electrodes (like the passive probes being developed by the Michigan group). In both of these cases the package is again another glass capsule that is electrostatically sealed to the silicon substrate. Notice that in this case, the glass package need not be a high profile capsule, but rather it need only have a cavity that is deep enough to allow for the silicon chip to reside within it. Note that although the silicon IC chip is originally 500μm thick, it can be thinned down to about 100μm, or can be recessed in a cavity created in the silicon substrate itself. In either case, the recess in the glass is less than 100μm deep (as opposed to several millimeters for the glass capsule). Such a glass package can be easily fabricated in a batch process from a larger glass wafer.

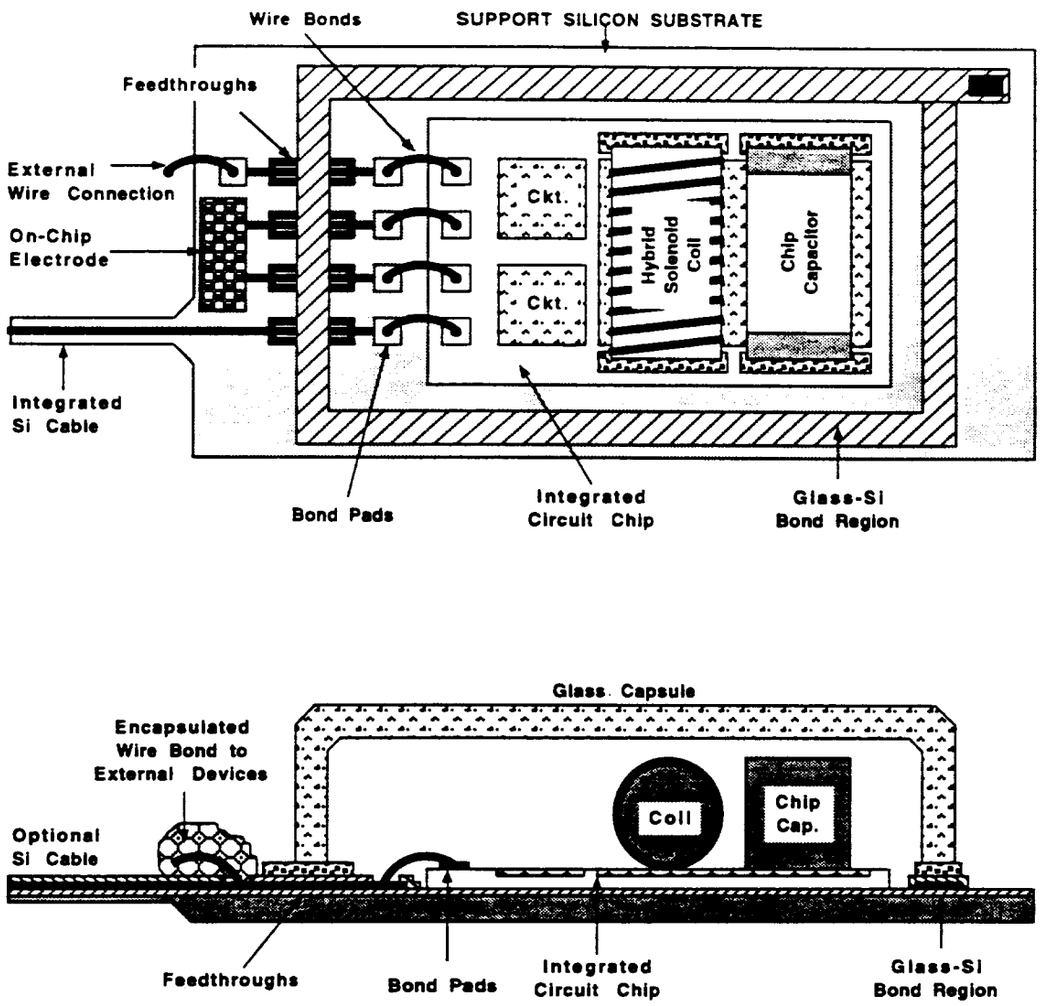

Figure 1: A generic approach for packaging implantable neural prostheses that contain a variety of components such as chip capacitors, microcoils, and integrated circuit chips. This packaging approach allows for connecting to a variety of electrodes.

We believe the above two approaches address the needs for most implantable neural prostheses. Note that both of these techniques utilize a silicon substrate as the supporting base, and are not directly applicable to structures that use other materials such as ceramics or metals. Although this may seem a limitation at first, we believe that the use of silicon is, in fact, an advantage because it provides several benefits. First, it is biocompatible and has been used extensively in biological applications. Second, there is a great deal of effort in the IC industry in the development of multi-chip modules (MCMs), and many of these efforts use silicon supports because of the ability to form high density interconnections on silicon using standard IC fabrication techniques. Third, many present and future implantable probes are based on silicon micromachining technology; the use of our proposed packaging technology is inherently compatible with most of these probes, which simplifies the overall structure and reduces its size.

Once the above packages are developed, we will test them in biological environments by designing packages for specific applications. One of these applications is in recording neural activity from cortex using silicon microprobes developed by the Michigan group under separate contracts. The other involves the chronic stimulation of muscular tissue using a multichannel microstimulator for the stimulation of the paralyzed larynx. This application has been developed at Vanderbilt University. Once the device is built, it will be used by our colleagues at Vanderbilt to perform both biocompatibility tests and functional tests to determine package integrity and suitability and device functionality for the reanimation of the paralyzed larynx. The details of this application will be discussed in future progress reports.

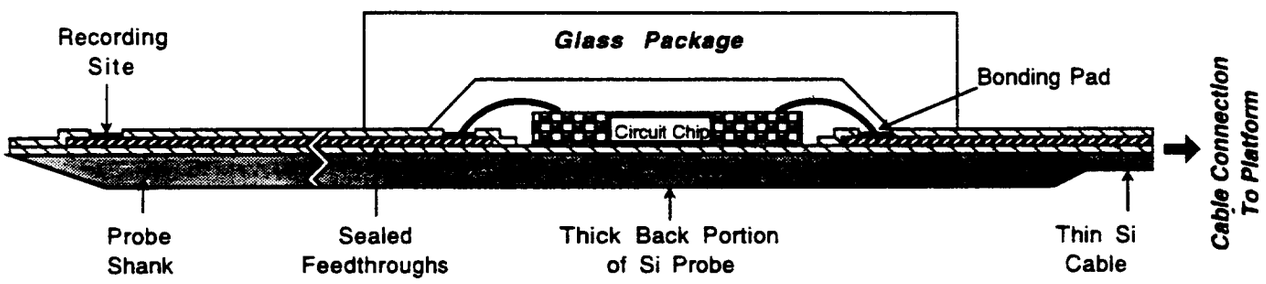

Figure 2: Proposed packaging approach for implantable neural prostheses that contain electronic circuitry, either monolithically fabricated in the probe substrate or hybrid attached to the silicon substrate containing microelectrodes.

2. ACTIVITIES DURING THE PAST QUARTER

2.1 Hermetic Packaging

Over the past few years we have developed a bio-compatible hermetic package with high density, multiple feedthroughs. This technology utilizes electrostatic bonding of a custom-made glass capsule to a silicon substrate to form a hermetically sealed cavity, as shown in Fig. 3. Feedthrough lines are obtained by forming closely spaced polysilicon lines and planarizing them with LTO and PSG. The PSG is reflowed at 1100° C for 2 hours to form a planarized surface. A passivation layer of oxide/nitride/oxide is then deposited on top to prevent direct exposure of PSG to moisture. A layer of fine-grain polysilicon (surface roughness 50Å rms) is deposited and doped to act as the bonding surface. Finally, a glass capsule is bonded to this top polysilicon layer by applying a voltage of 2000V between the two for 10 minutes at 320°C, a temperature compatible with most hybrid components. The glass capsule can be either custom molded from Corning code #7740 glass, or can be batch fabricated using ultrasonic micromachining of #7740 glass wafers.

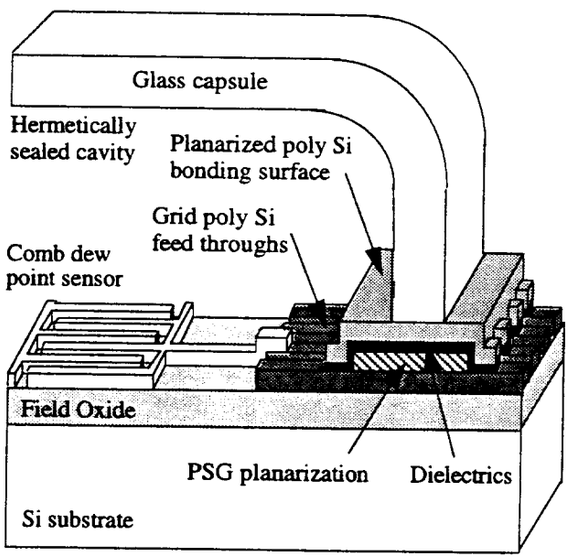

Figure 3: The structure of the hermetic package with grid feedthroughs.

During the past few years we have electrostatically bonded and soak tested over one hundred and sixty of these packages. The packages successfully prevent leakage in soak tests at 95°C for over 4 months on average and at 85°C for almost 9 months in deionized water. The bonding yield has varied between 85% to 72% (yield is defined as the percentage of packages which last more than 24 hours soaking in DI water), and preliminary in-vivo tests indicate that the package is bio-compatible and rugged. We also would like to mention that the earlier tests that have been going for more than a year (room temperature soak tests in saline and the 85°C and the 95°C tests in deionized water) have been made with silicon substrates that are thinned (~150μm) and using the custom made glass capsules. The relatively newer tests (85°C and 95°C tests in saline) are performed with the silicon substrates having full thickness (~500μm) and the improved glass capsules with the flat top surface.

2.1.1 Accelerated Soak Tests Of Ultrasonically Machined Glass Capsules.

One of the issues that needed to be addressed and was raised in the past was whether the improved glass packages bonded to full thickness silicon substrates were hermetic. During this quarter we have soak tested 28 of these packages under accelerated conditions in saline solutions and our results indicate that these packages are hermetic. The most important advantage of these packages is (since they are bonded to thicker substrates) the fact that they are mechanically stronger and could survive longer periods in actual implants. These results are particularly encouraging in spite of the fact that the bonding surfaces of these silicon substrates were not as planar as desired, which was caused by improper etching of the polysilicon feedthroughs. Another major accomplishment of this quarter was that for the first time in our soak tests we have performed accelerated tests (namely temperatures 85°C and 95°C) using phosphate buffered saline and verified that our packages stay hermetic for a calculated mean-time-to-failure of 22.7 years at body temperature.

We discussed in our last progress report that we fabricated 28 test packages using the improved glass capsules and full thickness silicon substrates. We have soaked 17 of these packages at 85°C and the remaining 11 packages at 95°C in phosphate buffered saline . Tables 2 and 3 list some pertinent data for these soak tests. Figure 4 summarizes the final results from the 95°C soak tests and Figure 5 summarizes the results obtained so far from the 85°C soak tests. One important property of these packages is that they are mechanically stronger than the previous packages and as such the handling losses have been reduced down to zero in both soak tests. The figures show a curve fit to our lifetime data that illustrates the general trend.

Table 2: Key data for 85°C soak tests in saline.

Number of packages in this study	17
Soaking solution	Saline
Failed within 24 hours (not included in MTTF)	3
Packages lost due to mishandling	0
Longest lasting packages so far in this study	188 days
Packages still under tests with no measurable room temperature condensation inside	6
Average lifetime to date (MTTF)	*84.9 days*

Table 3: Key data for 95°C soak tests in saline.

Number of packages in this study	11
Soaking solution	Saline
Failed within 24 hours (not included in MTTF)	5
Packages lost due to mishandling	0
Longest lasting packages so far in this study	70 days
Packages still under tests with no measurable room temperature condensation inside	0
Average lifetime to date (MTTF)	*38 days*

From the 17 packages that we have started at 85°C, 3 failed within a day, indicating major surface defects or poor alignment of the glass capsule to the silicon substrate. From the remaining 8 packages that were tested in the beginning of this quarter, only 2 failed during this quarter. One of these packages lasted for 40 days and the other one failed after 99 days. We define failure as room temperature condensation. The packages in these accelerated tests have been monitored every few days for room temperature condensation both electrically by means of an integrated dew point sensor and by visual inspection with the use of a microscope. We have noticed that if we do not change the solution regularly, the water in the saline containers that house the packages slowly evaporates and hence the saline solution becomes more concentrated. This, not only leaves a residue on the glass causing difficulty in visual inspection, but also enhances dissolution. As such, in order to improve the lifetimes of these packages we have been replacing the saline solution every day. Of these packages the longest one lasted for 188 days with no sign of moisture. The second longest lasting sample has reached a total of 154 days. In addition to these there are 2 more samples at 104 days and an additional 2 at 103 days all showing no signs of moisture. The oldest sample has apparent dissolution along the outer periphery of the bonding surface, but it is not wide enough to penetrate into the package. The other samples that have reached 103 and 104 days have significantly less corrosion as expected. We relate these differences to the variations in the bond strength around the outer perimeter of the bonding region and also the possibility of surface nonuniformities. From this data we have calculated a worst case mean time to failure based on the assumption that all the samples fail today and found a mean time to failure of 84.9 days.

From the 11 samples that were started at 95°C, five failed during the first day of testing most likely due to alignment problems and also due to surface defects. From the remaining 6 samples that were tested during this quarter, unfortunately all have failed. The main reason for these failures is the fact that dissolution is exponentially related to temperature and as such the failures at 95°C soak tests occur much sooner. After inspecting the failed samples, we have observed major dissolution of the bonding surface starting from the outer perimeter of the bonding surface and penetrating into the package as mentioned and displayed in our past progress report. The fact that all the samples contain at least one leakage path across the bonding surface helps us to identify our failure modes. With this data our calculated mean time to failure turned out to be 38 days with the longest lasting sample surviving for 70 days. The other packages have lasted for 20, 23, 29, 39 and 47 days. We are also confident that the nonplanar bonding surface has been another factor for the faster penetration of saline into these packages. Later, we fabricated three new packages and have coated them with a biocompatible epoxy and then soaked them in 95° C. Since the packages have been treated differently we did not include these results in the above-mentioned 11 samples. So far these 3 packages are dry both electrically and visually after soaking 51 days in saline at 95°C. In addition to this, their bonding surfaces show minimal dissolution. Both of these factors indicate that the epoxy was useful in acting as a barrier to the corrosion of the polysilicon surface by the saline solution. The only drawback is that air gets trapped between the epoxy and the glass silicon interface during the application of epoxy and when the package is raised to higher temperatures in saline, the air expands and forms bubbles. We hope to improve our method in applying epoxy and will try to use a different epoxy to protect the bonding surface from saline. We have started the fabrication of new silicon substrates and hope to reduce the nonplanarity of the bonding surfaces and as such hope to improve the lifetime of our packages. In addition, we hope to be able to perform additional tests at lower temperatures than 95°C in order to avoid the use of epoxy altogether and still be able to obtain accelerated test data. In order to do this we need to expand our test facilities which we hope we will be able to do in the next few months.

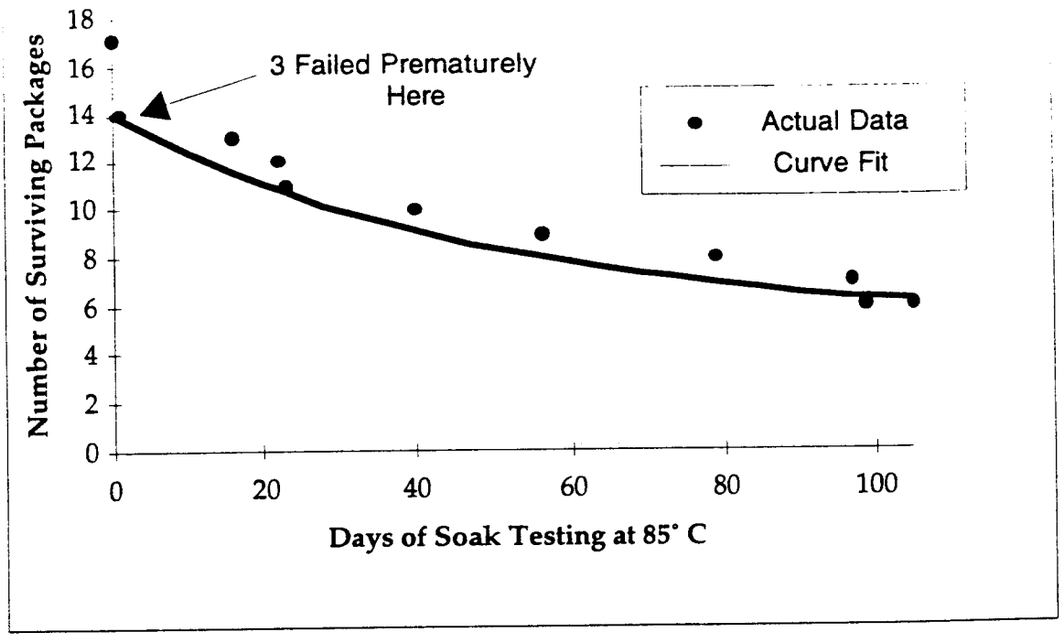

Figure 4: Summary of the lifetimes of the 17 packages which have been soak tested at 85° C in saline solution.

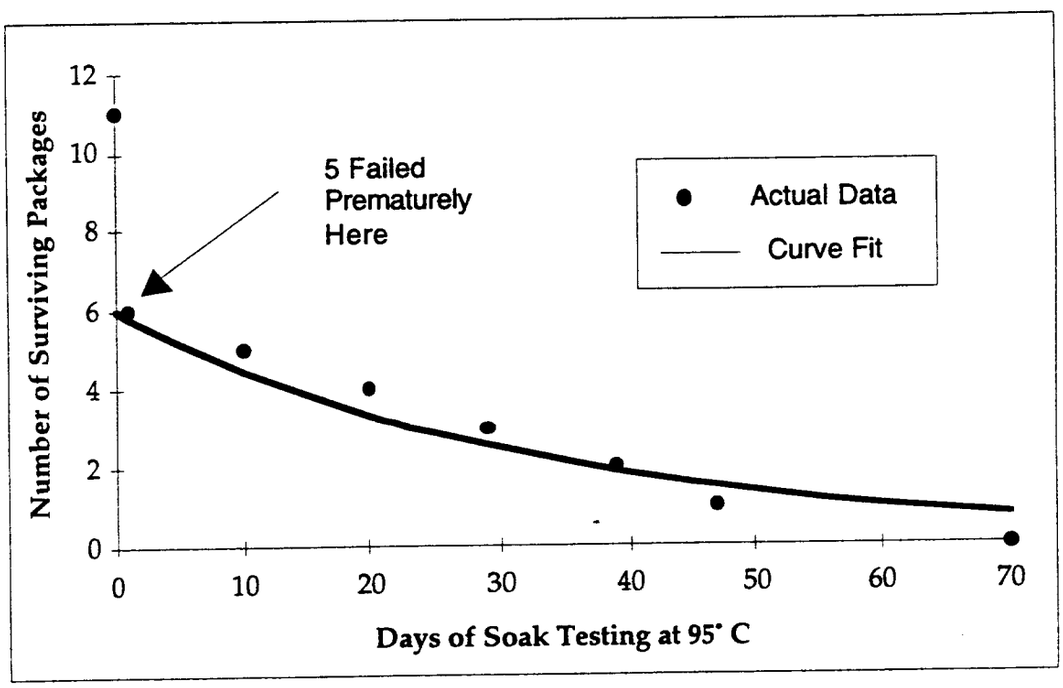

Figure 5: Summary of the lifetimes of the 11 packages which have been soak tested at 95° C.

2.1.2 Interpretation of the Long Term Soak Test Results in Saline

As was discussed in previous progress reports, we can model the mean time to failure (MTTF) as an Arrhenius processes (In the VLSI industry this model is used for failure due to diffusion, corrosion, mechanical stress, electromigration, contact failure, dielectric breakdown, and mobile ion/surface inversion). The generalized equation used in all these cases is given below where MTTF is the mean time to failure, A is a constant, ξ is a stress factor other than temperature (such as pressure or relative humidity), n is the stress dependence, Q is the activation energy, K_B is Boltzman's constant, and T is the temperature in Kelvin:

$$MTTF = A \cdot \xi^{-n} \cdot e^{\left(\frac{Q}{K_B T}\right)}$$

For the accelerated soak tests that we have performed on the packages, there was no stressing factor other than temperature, so the ξ term drops out of the above equation. The resulting equation can be rewritten as a ratio of MTTF's as it is below. This is the model we are using to interpret the accelerated soak tests:

$$AF = \frac{MTTF_{Normal}}{MTTF_{Accelerated}} = e^{\frac{Q}{K_B}\left(\frac{1}{T_{Normal}} - \frac{1}{T_{Accelerated}}\right)}$$

By using the current MTTF's at 85°C and 95°C, we can easily calculate the activation energy (Q) and from this activation energy we can proceed to obtain an acceleration factor (AF) for these tests, and then calculate the MTTF at body temperature. Since the tests at 85°C are still in progress we cannot accurately determine the activation energy in our tests. Also until all of the samples show leakage, we cannot obtain the MTTF at the accelerated temperatures. We can, however, obtain worst case MTTF's for the 85°C soak tests by assuming that all the remaining packages in this test show leakage today. This worst case MTTF can be used to calculate the worst case activation energy, and hence the worst case MTTF at body temperature. Performing this calculation yields:

$$MTTF|_{85°C} = 84.9\,Days \qquad MTTF|_{95°C} = 38\,Days$$

Q=0.913eV, AF(95°C)=218, AF(85°C)=97.6

$$MTTF|_{37°C} = 22.7\,Years$$

We call this average lifetime at body temperature of 22.7 years the worst case lifetime because every extra day that the remaining 85°C packages last increases this projected lifetime. The above activation energy of 0.913eV is about what we expect for these packages. For comparison, corrosion is known to be one of the major failure mechanisms for plastic-encapsulated silicon chips, and the activation energy for corrosion of these standard plastic packages is well characterized and known to be about 0.7 to 0.9 eV.

2.1.3 Ongoing Accelerated Soak Tests in Deionized Water

We have continued accelerated soak testing of the old glass packages this quarter, and 25% of the packages in these tests have now surpassed one year of accelerated testing with 20% still showing no signs of moisture penetration. For these tests we have chosen temperature as the acceleration factor because it is an easy variable to control, and because moisture diffusion is a strong (exponential) function of temperature. We started our tests by soaking 10 samples each at 95°C and 85°C. Tables 4 and 5 list some pertinent data for these soak tests. Figure 6 summarizes the results so far from the 95°C soak tests and Figure 7 summarizes the results so far from the 85°C tests. These figures also list the causes of failure for individual packages when it is known, and they show a curve fit to our lifetime data to illustrate the general trend. The curve fit, however, only approximates the actual package lifetimes since some of our packages failed due to breaking during testing rather than due to leakage. We should mention that the handling failures occurred mainly during the first few months of the tests and we have not observed any handling related failures after having gained expertise in testing these devices.

None of the ongoing packages in the 85°C soak tests failed this quarter. The only package being tested at 95°C failed due to complete dissolution of the silicon substrate from the back side. As mentioned before, the silicon substrate dissolves away slowly at the higher temperature and we had noticed that the one sample soaking at 95°C had been getting thinner and expected it to fail any time. It did fail this past quarter and it was interesting to see that almost all of the silicon substrate had etched away. The packages in these accelerated tests have been monitored every few days for room temperature condensation both electrically by means of an integrated dew point sensor, and by visual inspection microscopically. Of the original 10 packages in the 95°C tests, the longest lasting package survived for a total of 484 days. The calculated mean time to failure of the packages is 135.7 days excluding the handling errors. Of the original 10 packages in the 85°C soak tests there are still 4 with no sign of room temperature condensation with the longest one lasting more than 506 days. The worst case mean time to failure for these tests have been calculated as 396 days excluding the handling errors.

2.1.4 Interpretation of the Long Term Soak Testing Results in Deionized Water

Similar to the model we have used in our accelerated soak tests in saline, by using the current MTTFs at 85°C and 95°C, we can easily calculate the activation energy (Q) and from this activation energy we can proceed to obtain an acceleration factor (AF) for these tests, and then calculate the MTTF at body temperature. Since the tests in 85°C are still in progress we cannot accurately determine the activation energy in our tests. Also until all of the samples show leakage, we cannot obtain the MTTF at the accelerated temperatures. We can, however, obtain worst case MTTFs for the 85°C soak tests by assuming that all the remaining packages in this test show leakage today. This worst case MTTF can be used to calculate the worst case activation energy, and hence the worst case MTTF at body temperature. Performing this calculation yields:

$$MTTF|_{85°C} = 257.4\,Days \qquad MTTF|_{95°C} = 118.7\,Days$$

Q=0.8795eV, AF(95°C)=178.5, AF(85°C)=82.3

$$MTTF|_{37°C} = 58\,Years$$

This average lifetime at body temperature of 58 years is the worst case lifetime because every extra day that the remaining 85°C packages last increases this projected lifetime. Also, it should be noted that we have included every single sample in the 85°C and 95°C soak tests in this calculation except the 15% which failed in the first day (we assume that these early failures can be screened for). However some of these capsules failed due to mishandling during testing, rather than due to actual leakage of the package. If we disregard the samples that we have attributed failure to mishandling, we obtain a somewhat longer mean time to failure:

$$MTTF|_{85°C} = 396\,Days \qquad MTTF|_{95°C} = 135.7\,Days$$

Q=1.217 eV, AF(95°C)=1304, AF(85°C)=447

$$MTTF|_{37°C} = 485\,Years$$

The above activation energy of 1.217eV is a little higher than what we expect for these packages mainly because of the fact that for standard plastic packages it is typical to have activation energies about 0.7 to 0.9 eV. These results clearly indicate that both types of glass capsules provide protection against moisture penetration for at least a few years. Obviously as we collect additional test data we will be able to better estimate the MTTF.

Table 4: Key data for 95°C soak tests in DI water.

Number of packages in this study	10
Soaking solution	DI water
Failed within 24 hours (not included in MTTF)	1
Packages lost due to mishandling	2
Longest lasting packages in this study	484 days
Packages still under test with no measurable room temperature condensation inside	0
Average lifetime to date (MTTF) including losses attributed to mishandling	*118.7 days*
Average lifetime to date (MTTF) not including losses attributed to mishandling	*135.7 days*

Table 5: Key data for 85°C soak tests in DI water.

Number of packages in this study	10
Soaking solution	DI water
Failed within 24 hours (not included in MTTF)	2
Packages lost due to mishandling	3
Longest lasting packages so far in this study	506 days
Packages still under tests with no measurable room temperature condensation inside	4
Average lifetime to date (MTTF) including losses attributed to mishandling	*257.4 days*
Average lifetime to date (MTTF) not including losses attributed to mishandling	*396 days*

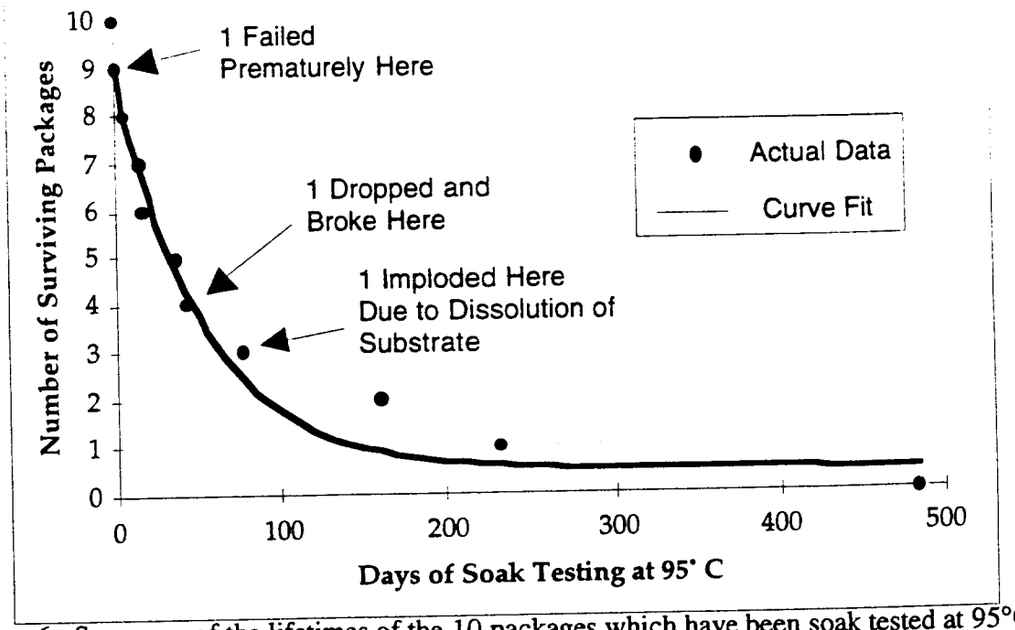

Figure 6: Summary of the lifetimes of the 10 packages which have been soak tested at 95°C in DI water.

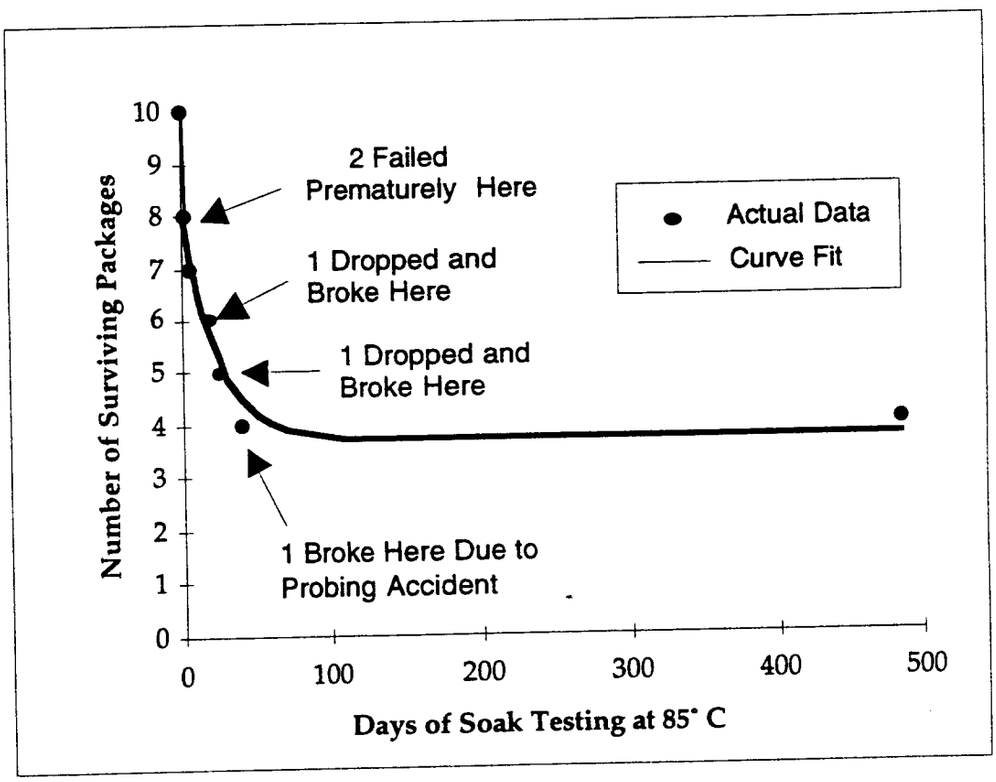

Figure 7: Summary of the lifetimes of the 10 packages which have been soak tested at 85°C in DI water.

2.1.5 Ongoing Room Temperature Soak Tests

During the past 13 months we have been soaking a group of packages in phosphate buffered saline at room temperature. Table 6 below lists some of the pertinent data from these soak tests. There were two main reasons for us to start these tests. First, we wanted tests done in saline. Secondly, we wanted some soak test data independent of the acceleration technique used. Admittedly, the room temperature tests will take a long time to produce meaningful data. However, the results obtained this way will act as a good control method to verify the overall integrity of our package.

We have soaked 6 packages in saline at room temperature. One of these packages leaked within a day, indicating surface defects or poor alignment of the glass capsule to the silicon substrate. Another one failed after 160 days of soaking. The remaining 4 packages have shown no sign of moisture either measured electrically or observed visually after an average of 393 days of soaking and are still under test.

Table 6: Data for room temperature soak tests in saline.

Number of packages in this study	6
Soaking solution	Saline
Failed within 24 hours (not included in MTTF)	1
Longest lasting packages so far in this study	393 days
Packages still under tests with no measurable room temperature condensation inside	4
Average lifetime to date (MTTF)	*343.2 days*

2.1.6 In-Vivo Tests

Last quarter we prepared and sent 8 packages to our colleagues at Vanderbilt University. These packages are made with the improved glass capsules and are bonded to thick silicon substrates. The results from these packages would be included in the next progress report. This quarter, we have also fabricated seven more of these dummy packages (with no active circuitry inside) and have sent them to another research group at Hines VA Hospital in Hines, Illinois (Dr. James Walter). We have been told that 2 of these 7 devices will be coated with a biocompatible epoxy to round up some of the sharp edges and corners. We look forward to receiving the results of these implants and will include more detailed discussion of these results in the next quarterly report.

2.2 Implantable Microstimulators

2.2.1 Progress Toward Single-Channel Microstimulator Delivery

We are preparing for delivery of microstimulator units in the near future, but there are certain obstacles that we are in the process of solving first. As detailed in last report, we have finished fabrication of a microstimulator wafer with a copper electroplated second metal layer. It is to this layer that we microweld the small receiver coils and attach the charge storage capacitors with conductive modified polyimide. We had initially had some trouble wire bonding the microstimulator chips to their respective electrode substrates, but with some slight modifications to the assembly process detailed in last report, we believe that we have overcome this problem consistently. The present single-channel microstimulator has been shown to work very well. The main problem that we are having now is in optimizing the telemetric link so as to be able to use moderate to large diameter external coils effectively and consistently with the microstimulator. That is, we have gotten good results from telemetrically powering the microstimulators, but the device has had to be operated within a limited range (1-2cm), fairly close to the edge of the external coil. Obviously it is desirable to be able to operate the devices anywhere within an external coil of useful size, and thus operated, to find that the devices respond as expected, are tolerant of misalignment within the external coil, etc. Solutions to this problem are being investigated before units can be delivered. We are developing and testing various mathematical models of the telemetry link in order to better understand the principal difficulties being encountered. Using these models, we hope that we will be able to optimize our telemetry link to be able to effectively power and control the microstimulator with a variety of external coil types and sizes.

Characterization Of Microstimulator's Performance

Using a tightly-coupled telemetric link to power the devices, several microstimulators were tested underneath our probe station to characterize the strength of the microstimulator's 8V and 4V supplies and maximum frequencies at which the clock and envelope detector / logic circuitry still respond. A single-ended DC voltage was also swept at the input to examine how the DC response of the supplies differs from the response observed when powered telemetrically. The input current drawn by the circuitry was also measured as a function of this DC input voltage. A weaker but more realistic link was used to study how well the microstimulator would drive varying output loads as received voltage conditions changed.

Figure 8 shows the response of the on chip supplies and the current drawn by the circuitry for these DC and telemetric tests. There are several significant points to be noted from this data. When telemetrically operated, the supplies consistently respond slightly below the values that would be expected from a single-ended DC input. This is probably because the average voltage seen after the rectification of the input sinusoid is lower than that seen when a DC input is applied. This to some extent is a function of the integrated capacitor across the rectifier bridge, that stabilizes the fluctuations seen across the bridge and supplies. This capacitor cannot easily be made much larger, since this would require an area tradeoff with other functions that must occupy space on the chip. Nonetheless, it shall be seen shortly that the principal effect of this reduction in the supplies is to limit the size of the load that can be driven at the desired 10mA current level. As for functionality in general, this depends more on the 4V supply from which the clock, envelope detector, and logic circuitry work. This 4V supply, too, is reduced when operated telemetrically versus with a DC single-ended input. Nonetheless, the 4V supply stays quite stable within a wide voltage range, approximately 8V to 20V, enabling the microstimulator to continue pulsing as expected. This effectively means that the received voltage peak should be at least 10-11V, since a modulation depth of at least 2V is desirable, and 3V would be preferable.

The clock was also studied, with a DC input voltage upon which was superimposed a fast periodic ripple. This was done because it was impossible to tune the microstimulator telemetrically to the range of frequencies that could be used with this first approach. The clock was found to work fine up to an input carrier of 20MHz, with the clock's output frequency being half of the carrier frequency.

The envelope detector was studied telemetrically, in the range of modulation frequencies (modulating with a square wave) and input voltages over which both it and the logic worked. Functionality of the envelope detector alone was not considered a valid criterion, since it is important that the logic circuitry be able to respond such that the device pulses as required. These results are summarized in Table 7. The worst case results, those for the lowest input voltage and corresponding lowest maximum modulation frequency, still mean that one would theoretically be able to address subsequent microstimulators in about (1/625) second, assuming a pulse duration of 200μs. The maximum stimulation rate for any single microstimulator still remains about 40-46Hz.

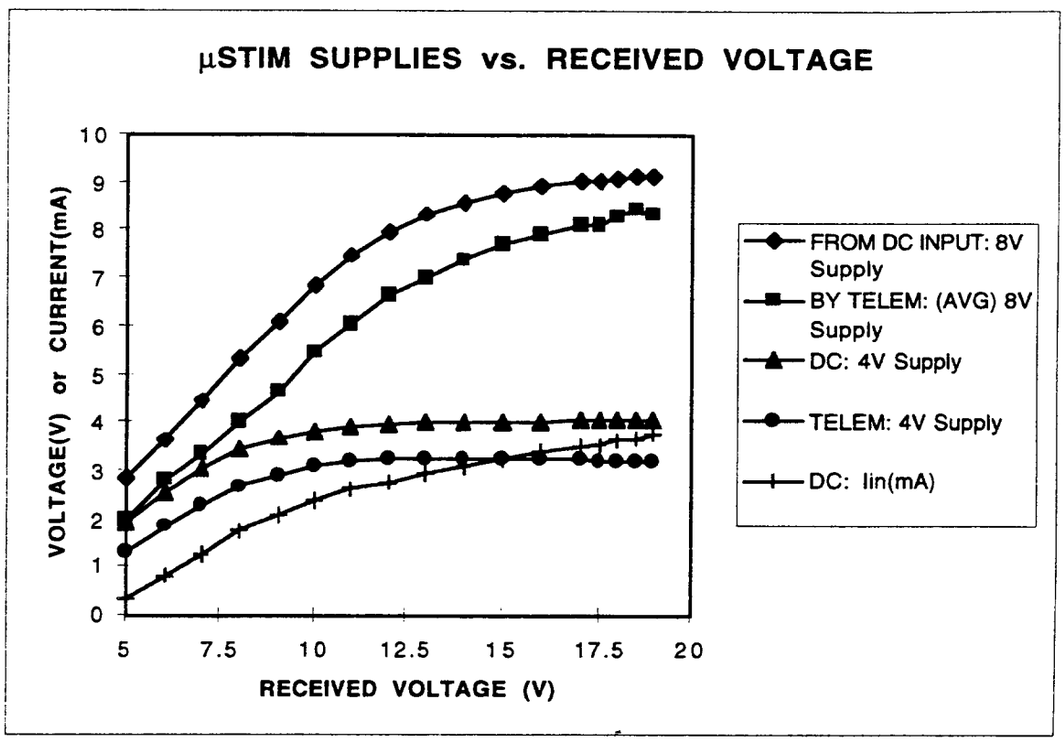

Figure 8: The Microstimulator's voltage supplies and input current drawn by the circuitry are plotted versus a single-ended DC input voltage and a telemetrically received voltage of the same amplitude.

Table 7: Using a square wave to modulate the telemetrically received signal, the maximum modulation frequencies at which the envelope detector and logic circuitry function well are shown for various input voltages.

INPUT VOLTAGE (V)	7.5 - 10.5	12 - 15.5	15 - 18
FREQ. RANGE fmod (kHz)	5	10	14.7

It can be seen that the microstimulator will operate over a wide range of input voltages, because the 4V supply on which the clock, envelope detector, and logic depend works well even when the 8V supply is considerably decayed from its maximum value. The 8V supply, however, will vary substantially over this input range. The net effect of this will be either a limit to the output load that can be driven at a stimulus current of 10mA or a limit to that stimulus current, below 10mA. The output stimulus circuitry is designed in such a way that the product of the stimulus current with the output load cannot exceed a voltage that is very close to the 8V supply voltage, i.e. $[I_{stim} * R_{load}] <= V_{8vSupply}$. Also, at sufficiently small 8V supply values, the current mirrors that create the output stimulus current and the recharge current will begin to fail, and the stimulus current will suffer accordingly. This does not imply that conversely, one can obtain currents much higher than 10mA by driving a sufficiently small load at a large enough 8V supply value. At high 8V supply values and low load values, the current will, however, be somewhat higher than 10mA. The results of these tests are shown in Table 8. It can be observed that the current generally starts at or near the 10mA expected strength, if the 8V supply voltage is capable of driving a particular load at 10mA initially. Then the current decays somewhat, in a fashion that can be shown to be essentially linear. The exceptions to this occur at high 8V supply voltages (i.e. high received voltages) and small loads (about 300Ω or below) or at lower 8V supply voltages and loads not much higher than 100Ω. All of the stimulus pulses were intentionally prolonged to 400µs instead of the more typical 200µs, although the microstimulator was given sufficient time to recharge between pulses. Thus, the decay in current levels observed here is worse than what can be expected in intended use of the microstimulator, because of this decay's linear characteristic.

Table 8: Summary of stimulus current results across varying loads, for various telemetrically received voltages. The stimulus current across various resistive loads is demonstrated for various telemetrically received voltage levels.

RECEIVED VOLTAGE (V)	LOAD RESIST. (Ω)	INITIAL CURRENT (mA)	FINAL CURRENT (mA)
8.5 -10.5	100	10	10
8.5 - 10.5	270	10	4
8.5 - 10.5	680	7.75 ±0.5	4.4
8.5 - 10.5	820	6	4.25
14 - 16	820	9.3	9.3
16 - 18.5	820	10.6	7.3
13 - 18	820	10	6.8
13 - 18	680	12	6.6
13 - 18	270	14.8	10

2.2.2 Multi-Channel Microstimulator

We have presented in detail the design and architecture of the second-generation, multichannel microstimulator (μstim-2) in previous progress reports. As has been discussed, μstim-2 has the ability to transmit data to the outside world using an on-chip transmitter and coil. In what follows we present the design and fabrication of this on-chip transmitter and coil.

On-Chip Transmitter Design

The on-chip transmitter designed for the microstimulator has a block diagram similar to the circuit of Figure 9, with an oscillator of the type shown in Figure 10. This oscillator is a basic ring oscillator with a NAND gate used in order to allow the oscillator to be turned on and off. Also, an extra capacitor, C_{del}, is included to introduce an added delay in the switching time for the NAND. This capacitance can be set by cutting programmable links and can allow the carrier frequency of the transmitter to be set after fabrication but before the device is put into operation. The main reason for using a basic ring oscillator is due to the frequency of operation that is desired for this transmitter. We want this transmitter to operate at as high a frequency (and data transmission rate) as possible, and a ring oscillator is the fastest type of oscillation circuit that can be fabricated.

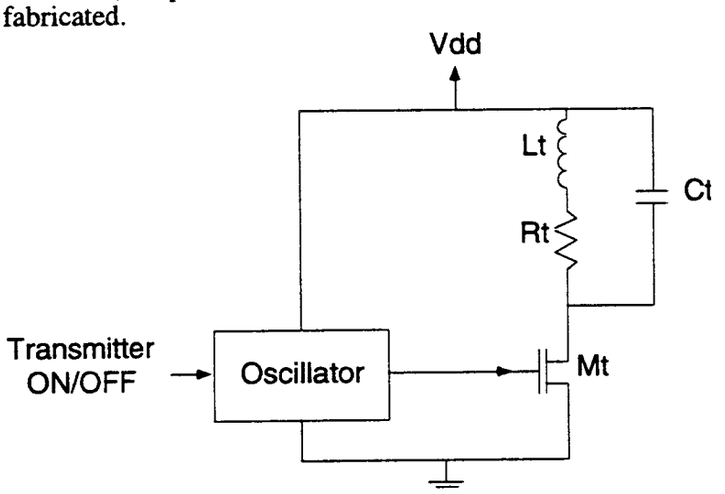

Figure 9: Block diagram for a transmitter using amplitude shift keying.

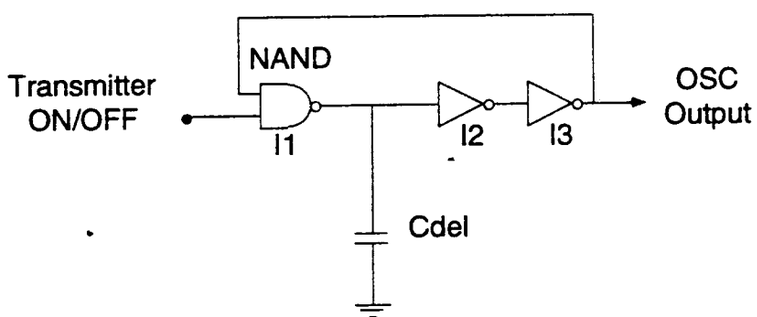

Figure 10: Circuit design for a ring oscillator with an ON/OFF switch.

The transmitter circuit for the microstimulator has been fabricated and is shown in Figure 11. It was simulated using various C_{del} and V_{dd} values and also tested experimentally. These results are given in Table 9, and Figure 12 shows a scope trace of the output voltage seen across a tuned L_tC_t tank circuit connected to the drain of the drive transistor M_t when an ON/OFF signal is sent to the transmitter. The difference between the measured and simulated results from variations in the parasitic capacitance, transistor W/L variations due to lithography, and k_p variations due to processing. Since the frequency can be set by cutting links on C_{del}, however, this difference does not pose any serious problems. The output trace shown in Figure 12 was measured while using a nickel electroplated on-chip coil, as is presented in the next section, with the parameters L_t=1.2μH, R_t=95Ω and a parallel tuned capacitance of C_t=16pF.

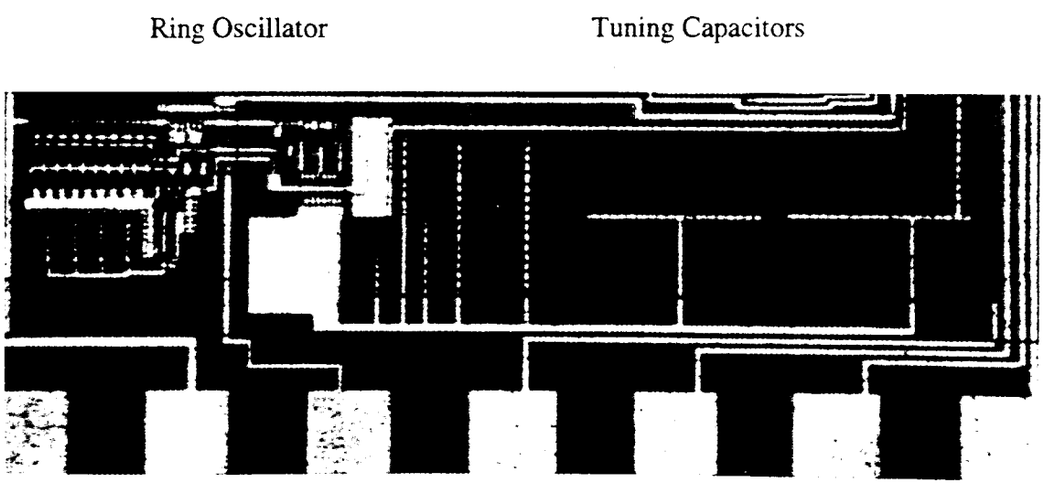

Figure 11: Fabricated circuit for the on-chip transmitter.

Table 9: Measured and simulated ring oscillator frequency.

Minimum oscillation frequency	20.4MHz (simulated)
Nominal oscillation frequency	28.4MHz (simulated) 32.9MHz (measured)
Maximum oscillation frequency	67.0MHz (simulated)
Change in frequency versus change in supply voltage	3.8MHz V^{-1} (with 9.5V supply)

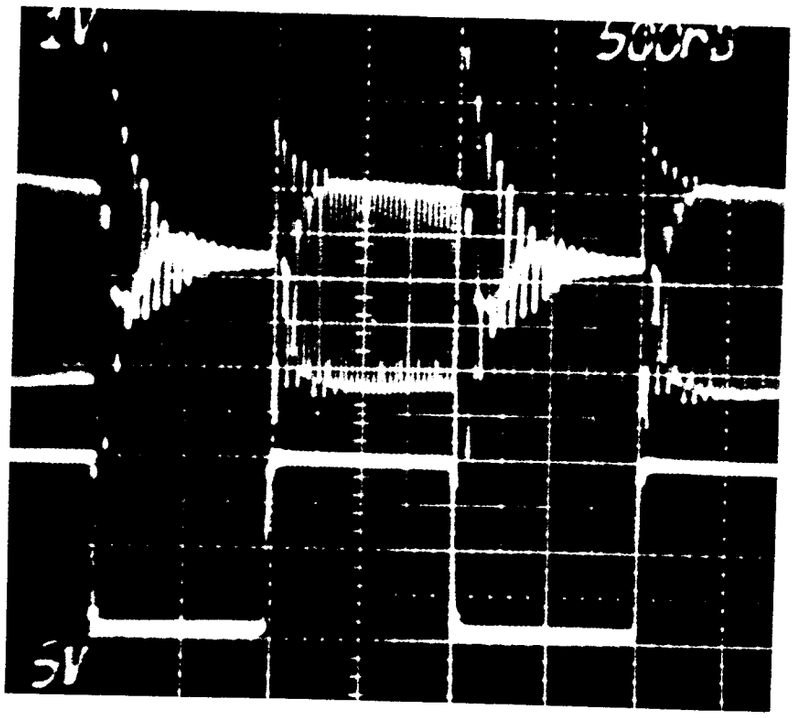

Figure 12: Measured output across the LC tank circuit of Figure 9 when a transmit ON/OFF signal is sent to the on-chip transmitter.

Transmitter Coil Characteristics And Fabrication Process

Along with having a stable oscillator for the on-chip transmitter, it is also extremely important to have a high quality inductor coil to use for transmitting the data. The inductor should have as high of an inductance value as possible, since this will increase the voltage that an external receiver will be able to pick up. The inductor should also be capable of operating at as high of a frequency as possible, to allow for as high of a data transmission rate as possible. Finally, as has been stated previously, the inductor should be fabricated on-chip, not as an external component that must be hybrid connected to the transmitter. This will allow the transmitter to have a much smaller size. Such an on-chip planar inductor will be similar to the one shown in Figure 13.

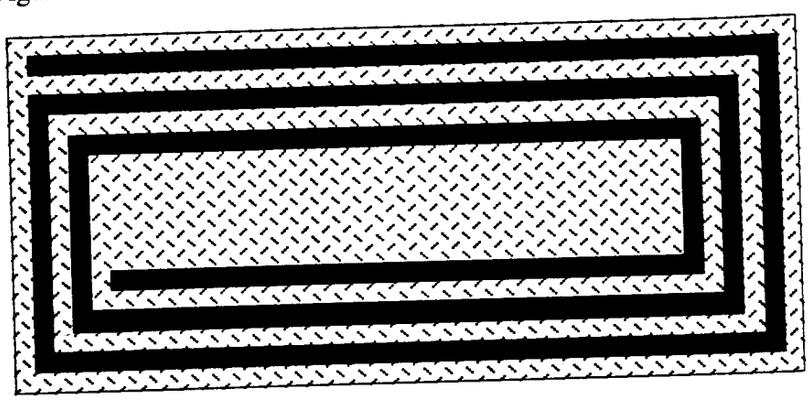

Figure 13: Basic design for a planar inductor coil.

This coil will have an inductance based on the number of turns, the coil width and length, the line size and spacing, and the relative permeability of the core. It will also have a parasitic series resistance based on the line material and dimensions, and it will have a parasitic parallel capacitance based on the line-to-line capacitance and the line-to-substrate capacitance. The equivalent circuit for the inductor is shown in Figure 14.

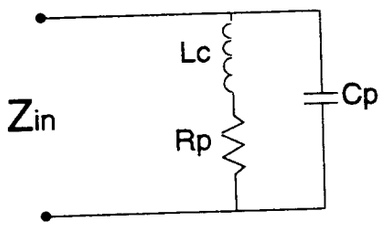

Figure 14: Equivalent circuit for a planar inductor

The circuit of Figure 14 can be evaluated for its impedance behavior versus frequency as:

$$Z_{in} = \frac{\left(R_p + j\omega L_c\right)\left(\frac{1}{j\omega C_p}\right)}{R_p + j\omega L_c + \frac{1}{j\omega C_p}} = \frac{R_p + j\omega L_c}{1 + R_p C_p - \omega^2 L_c C_p} \qquad (1)$$

Equation (1) has one zero and two poles, corresponding to the HPF effect of the RL combination, the LPF effect of the RC combination, and the parallel resonance of the LC combination. The coil should be fabricated so that the zero is lower in frequency than either pole. This would result in the frequency behavior shown in Figure 15, using the pole and zero frequency equations given in (2).

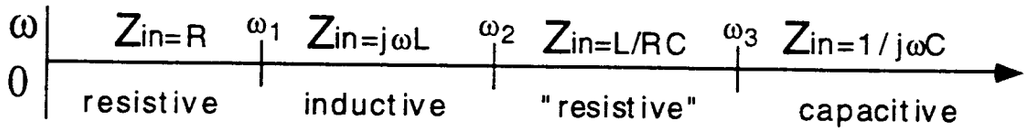

Figure 15: Frequency behavior for a well designed planar coil.

$$\omega_1 = \frac{R_p}{L_c}; \qquad \omega_2 = \frac{1}{R_p C_p}; \qquad \omega_3 = \sqrt{\frac{1}{L_c C_p}} \tag{2}$$

It can be seen from these equations that the coil resistance is a very important parasitic parameter. As the coil resistance increases, the HPF zero from RL will increase, and at the same time the LPF pole from RC will decrease. When the resistance becomes too high, the coil will not exhibit any inductive behavior at any frequency. The parasitic capacitance should also be kept small in order to keep the two pole frequencies high, but it is not as crucial. So, it is desirable to minimize the coil resistance and capacitance while trying to maximize the inductance.

For a planar coil with an air core, the inductance can be calculated from equation (3).

$$\begin{aligned} L_o = {} & 0.02339N^2\left[(s_1+s_2)Log\left(\frac{2s_1s_2}{ND}\right) - s_1Log(s_1+g) - s_2Log(s_2+g)\right] \\ & +0.01016N^2\left(2g - \frac{s_1+s_2}{2} + 0.447ND\right) - 0.01016N(s_1+s_2)(A+B) \end{aligned} \tag{3}$$

L_o = Inductance of a flat rectangular coil in microhenries
N = Number of turns of the coil
s_1 = Average length of side 1 of the coil in inches
s_2 = Average length of side 2 of the coil in inches
D = Line space plus line width in inches
$g = \sqrt{s_1^2 + s_2^2}$
A = Constant determined by the ratio of (d/D)
d = Cross sectional diameter of an individual coil winding in inches
B = Constant determined by number of turns in the coil

For the transmitter coil used in the multichannel microstimulator the dimensions of the coil sides, s_1 and s_2, were determined by the space available on the circuit chip. The inductance

value desired was determined by iterative solution of the inductance, parasitic resistance, and parasitic capacitance calculations in order to obtain a usable inductor in the range of operation of the transmitter (20-60MHz, as just presented previously). The parameters used for the coil are:

N=10, s_1=0.0488, s_2=0.292, D=0.000551, d=0.000492, g=0.296, A=0.452, B=0.266

For these given parameters, the inductance for the microstimulator transmitter coil can be calculated as:

$$L_o = 2.339[(0.3408)(0.714) - (0.0488)(-0.46) - (0.292)(-0.23)]$$
$$+1.016(0.592 - 0.1704 + 0.00246) - 0.1016(0.3408)(0.718) \qquad (4)$$

$$L_o = 0.779 + 0.431 - 0.0249 = 1.19\mu H$$

The parasitic resistance and capacitance for the coil can be found by equation (5), where the line width=line space=D/2, the thickness of the coil windings is H, and the thickness of the passivation oxide underneath the coil is t_{ox}.

$$R_p = \frac{\rho L}{A} = \frac{2\rho N(s_1 + s_2)}{H\left(\frac{D}{2}\right)}; \qquad C_p = \frac{\varepsilon A_{subst}}{t_{ox}} = \frac{\varepsilon_{ox}\varepsilon_0 ND(s_1 + s_2)}{t_{ox}} \qquad (5)$$

Using equations (4) and (2), along with the fact that we want the minimum operation frequency to be ≈20MHz, the maximum resistance that the coil can have is ≈125Ω. If that is used in equation (5), the minimum thickness that would be required for a coil made with aluminum is 5μm. This is much thicker than can be easily deposited using normal CMOS fabrication techniques. (i.e. - thermal or E-beam evaporation, sputtering, etc.) So, in order to achieve the low resistance required for a high inductance coil to be used at a frequency of 20-60MHz, an electroplating process using thick photoresist was developed.

The basic fabrication procedure that was developed for the low resistance, thick inductor coils is shown in Figure 16. This process consists of first taking the CMOS circuit and passivating it with an LTO or polyimide layer of >2μm. This passivation layer is then patterned with via holes where the inductor will make a connection to the CMOS circuit. Next an electroplating base is deposited over the entire wafer. This will act as the seed material for electroplating and will also provide a path for the electric current flow that is necessary for electroplating. After depositing the electroplating base, a thick photoresist mold is formed on the wafer. The thick photoresist can be spun, exposed, and developed similar to other, thinner resists. Patterning the photoresist is followed by electroplating a metal such as nickel, gold, or copper, into the open areas of the photoresist mold. Finally, the photoresist is removed, and then the electroplating base is removed from the areas of the wafer that were not electroplated. The most important feature of this electroplating fabrication process is that it is fully compatible with standard CMOS. It can be done after the CMOS processing is completed and requires no high temperature or other special steps. Also, it only requires the use of one mask, to pattern the photoresist, and the entire photoresist and electroplating process can be completed in one day. Figure 17 shows a typical cross section from a wafer that has been patterned with this thick photoresist process, but before electroplating. The resist is 16μm thick for this sample, and the aspect ratio is 17:1.

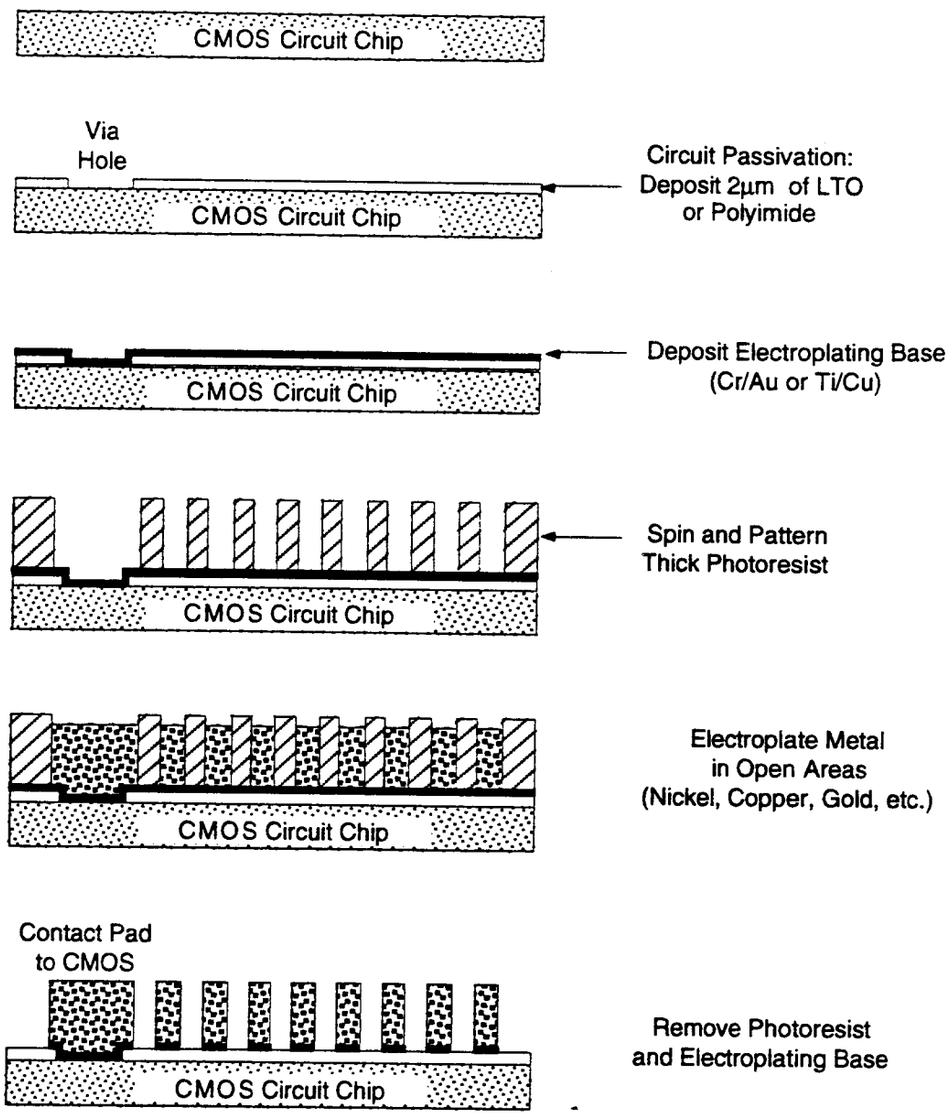

Figure 16: Electroplated coil fabrication process.

Figure 17: 16µm thick photoresist patterned using contact lithography

Using this process of thick photoresist and electroplating, it is possible to construct coils that are >15µm thick and that have a much lower resistance than is possible using normal CMOS metal deposition techniques. Coils of this type were fabricated using both nickel and copper as the electroplated metal, and the results are given in Table 10.

Table 10: Results obtained from a 15µm thick electroplated coil.

	Calculated	Measured
Lt	1.19µH	1.2µH
Cp	15pF	10pF
Rp (nickel)	40Ω	90Ω
Rp (copper)	13Ω	36Ω

The agreement between the calculated and measured values given in Table 10 is very good, especially the inductance. The difference in the capacitance value is likely due to a extra fringing fields that were added in the calculations, along with differences in the passivation oxide thickness. The resistance differences are due to the quality of electroplated metals. The calculated values were done assuming pure, high quality metal, but electroplated metals tend to not be as dense and so the resistance will be higher than would be expected for pure deposited films of the same thickness. Still, the resistance obtained for the copper coil is definitely low enough to provide a useful frequency range for the inductor. Using a copper coil as given in Table 10, the zero, pole, and resonant frequencies are: w_1=4.8MHz; w_2=442MHz; and w_3=46MHz. It can be seen that the RC pole can be neglected, and the usable operating range for this coil is from 4.8-46MHz. This type of copper electroplated coil has been successfully fabricated on top of a completed CMOS wafer, and an SEM photograph of the coil and circuitry is shown in Figure 18.

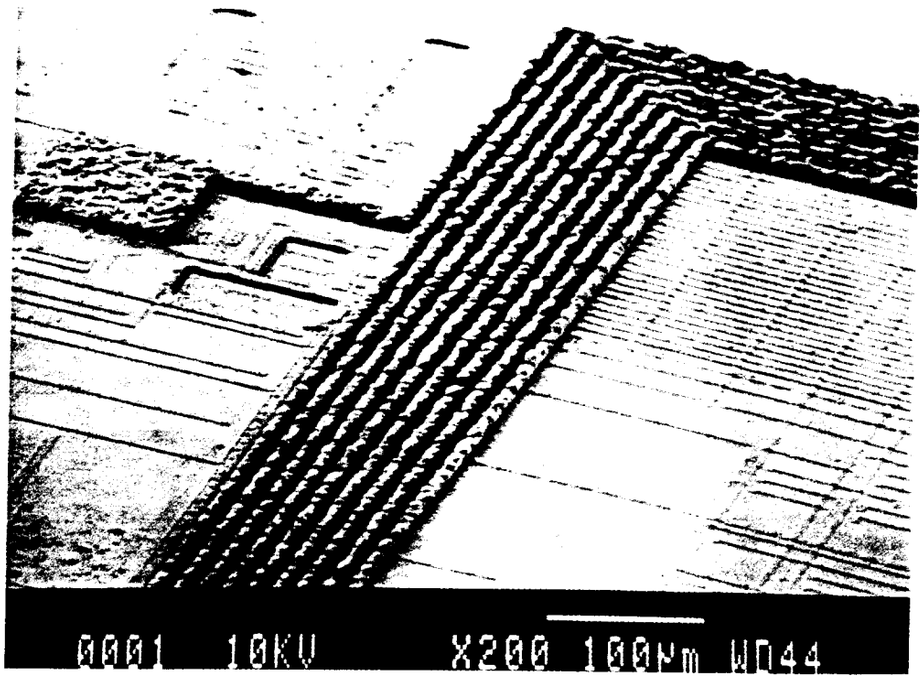

Figure 18: A ≈12µm thick copper coil electroplated on top of the microstimulator circuitry.

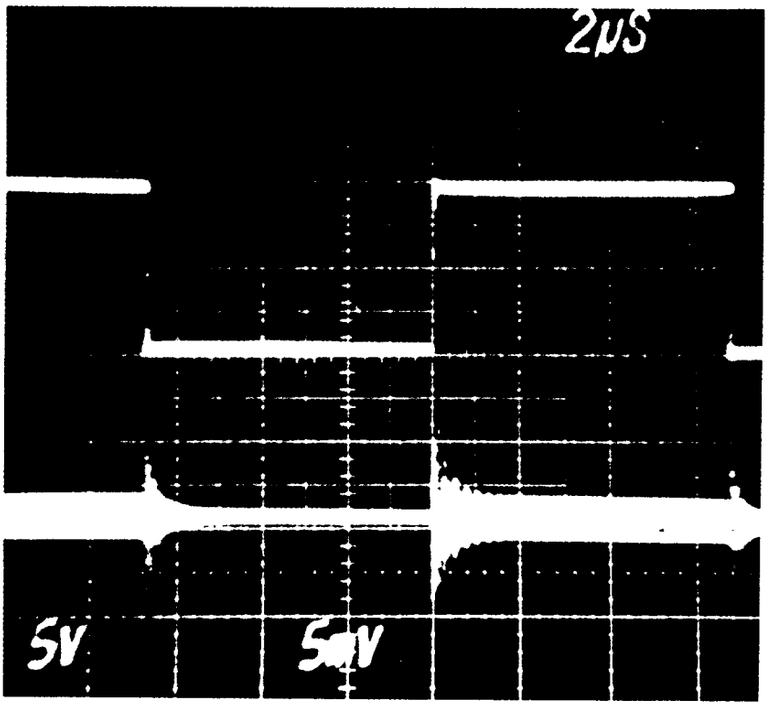

On-chip
Transmitter ON/OFF

Unfiltered Received Voltage

Figure 19: Unbuffered and unfiltered voltage received from a receiver coil
2 feet away from an on-chip transmitter.

External Receiver Circuitry

After designing the on-chip transmitter circuit and antenna coil, the signal that it transmits must be capable of being detected by the external controller. This task can be very challenging, especially since the external class E transmitter provides a relatively huge noise signal at 1.8MHz. Any external receiver circuit must be capable of detecting the signal transmitted by the on-chip transmitter, while filtering out the signal from the class E power transmitter. In order to make this filtering easier, it is desirable to have the on-chip transmitter and class E transmitter have as large of a frequency difference as possible. This is an additional reason to make the on-chip transmitter frequency as high as possible.

Some initial testing of the on-chip transmitter was done using a nickel coil. The maximum operating frequency for this coil is given in the previous section, and is determined by its self-resonance to be 46MHz. Since this frequency can vary slightly from one coil to another, some additional parallel capacitance was added in order to tune the resonance to a more stable and predictable operating point of 33MHz. The transmitter was then tuned and operated with this coil, and Figure 19 shows a photograph of an unbuffered and unfiltered 33MHz ASK voltage received with an external coil ≈2 feet away from the on-chip transmitter coil.

The received signal shown in Figure 19 is ≈4mV in amplitude and is very easy to detect by itself, but this measurement was made without the class E transmitter being turned on. If the class E transmitter is turned on, the received voltage becomes washed out by a 1.8MHz sinusoid with an amplitude of ≈2V. This is about 500 times the amplitude of the signal that is to be detected. In order to detect the on-chip transmitter signal in the presence of this large noise source, the signal must be filtered and amplified. Figure 20 shows a block diagram of the circuit that was used to detect the on-chip transmitter signal while operating in the presence of noise, such as the class E transmitter.

The received RF signal is first sent through a bandpass filter that is used to cut down noise sources at any frequency other than the on-chip transmitter frequency. This signal is then mixed with the output of an external oscillator in order to produce an intermediate frequency (IF) that is the difference between the two, and the result is sent through a high Q ceramic filter. The output of the ceramic filter is sent though a gain stage to a quadrature detector whose output is dependent on the difference between the frequency that is sent to it and the frequency that the quadrature tank circuit is tuned to. Finally, the output of the quadrature detector is sent to a comparator to provide the output data signal.

There are several points that should be noted about the circuit of Figure 20. First, the oscillator, mixer, limiter, quadrature detector, and comparator were all part of an MC3356 monolithic IC chip manufactured by Motorola, intended for use as a wideband FSK receiver. The LC tank and QUAD tank are provided by using external LC components. The bandpass filter is also provided externally. This block was implemented using a tuned LC followed by a cascade of four RC high pass filters. From simulations, this filter should provide factor of 22,000 in reduction of the 1.8MHz class E transmitter signal in comparison to a 30MHz signal received from the on-chip transmitter. The mixer is normally used in order to reduce the input RF signal to a frequency that can be handled better by the following amplifier stages without encountering instability in the circuit.

The circuit shown in Figure 20 has been tested along with the on-chip transmitter and coil and was able to detect the data transmitted, even in the presence of the noise introduced when the class E transmitter was turned on. It did not perform exactly as designed, however. It was found that the receiver only provided the proper output when the input RF signal was at a frequency that matched the ceramic filter frequency. This is a standard IF of 10.7MHz. From this observation, it seems likely that there is something wrong with either the oscillator or the mixer

in the front end of the receiver circuit, but it was not possible to obtain 100% verification of this conclusion. The operating point of the on-chip transmitter was retuned to 10.7MHz and the detection circuit was then able to provide the proper output data signal. Figure 21 shows the output from the external receiver when the on-chip transmitter is operating without the class E transmitter, and Figure 22 shows it operating at the same time as the class E transmitter. In both cases, the power and data signal for the on-chip transmitter are being sent from external sources. The on-chip transmitter is not being powered by the on-chip supplies. This was done to make the test setup much simpler. Also, as was presented previously, the oscillator for the on-chip transmitter was designed to operate over a frequency range of 20-67MHz. In order to have the on-chip transmitter operate at 10.7MHz, the supply voltage to the oscillator had to be reduced to approximately 1/2 of the voltage that the on-chip regulator would supply.

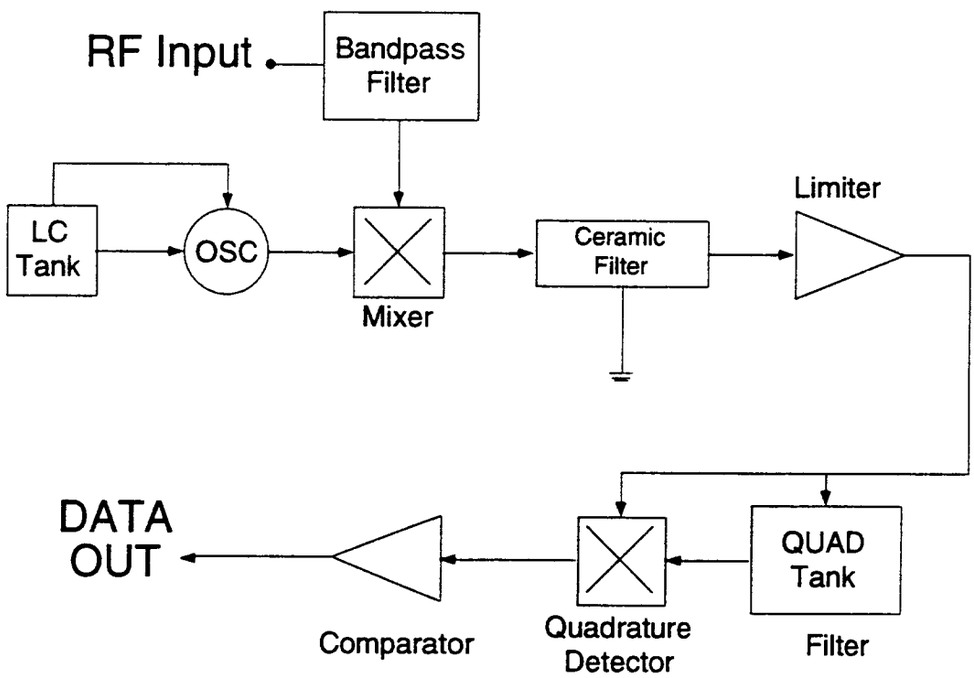

Figure 20: Receiver circuitry used by the external controller to detect the signal sent from the on-chip transmitter.

In addition, the data reception rate of the receiver circuit was limited. The receiver was only able to detect the data if it was transmitted at a bit rate of ≤100kHz. There should be more work done on this circuit block in the future in order to achieve better results. Since the Motorola IC used in this receiver was intended for use in wideband FSK systems, it is suggested that a completely new receiver design should be investigated for detecting the ASK signal sent from the microstimulator. This design could simply consist of several general RF amplifier stages, along with passive filters for providing a bandpass filter around the desired carrier frequency. The output of the RF amplifiers could then be peak detected and sent though a comparator. This type of system was not used originally for the receiver since using higher frequency RF amplifiers will make it more difficult to eliminate self-oscillations in the receiver. Hopefully, this work will be carried out in future quarters.

2.2.3 Data Transmission Errors in Inductively Coupled Links

As stated previously, it is very important that the microstimulator be as reliable as possible. In addition to circuit functionality, the reliability of the microstimulator also depends on the transmission of data to the device. Any noise in the communication could introduce errors in the received data. Figure 23 shows some sources of noise that could be introduced into the data transmission for the microstimulator RF telemetry system. These noise sources include: RF noise; introduction of loading on the transmitter coil from external objects (i.e. - ferrite materials); misalignment of the receiver coil in the X, Y, Z, or Ø angle direction; or warping of the transmitter coil causing possible detuning of the transmitter from the ideal tuned frequency. It is desirable to determine which, if any, of these types of errors will be most likely to occur in normal operation of the microstimulator. If it is known that a certain type of error might occur most frequently, steps can be taken to reduce the cause of this effect. For example, if coil warping is causing most errors, the transmitter coil can be made to be less flexible, or if RF noise is causing errors, the transmitter coil can be provided with additional shielding to eliminate it. This section details work done in testing a microstimulator data detection circuit while trying to simulate errors that could be introduced in actual operation.

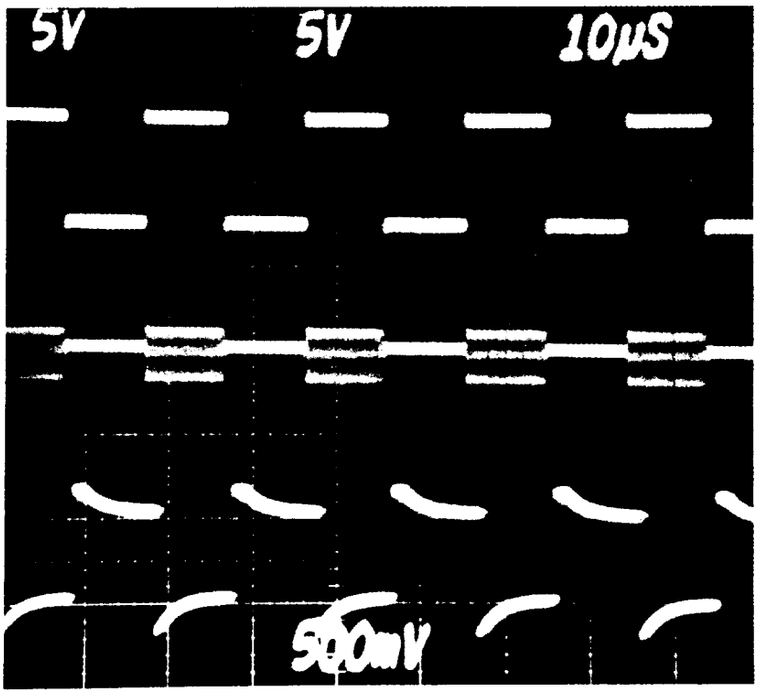

Figure 21: Output of the external receiver circuit for a signal sent using the on-chip transmitter and coil (with the class E transmitter OFF).

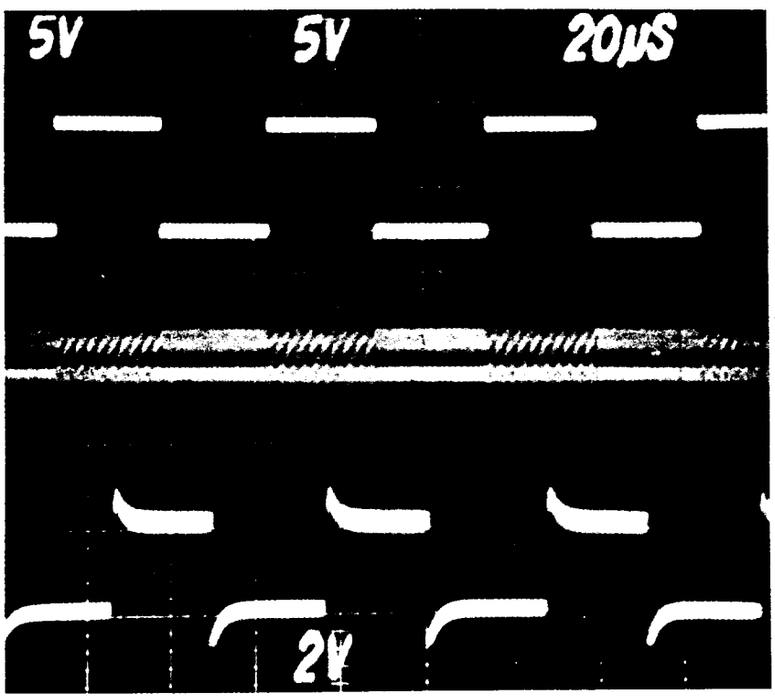

Transmitted data

Received signal

Received data output

Figure 22: Output of the external receiver circuit for a signal sent using the on-chip transmitter and coil (with the class E transmitter ON).

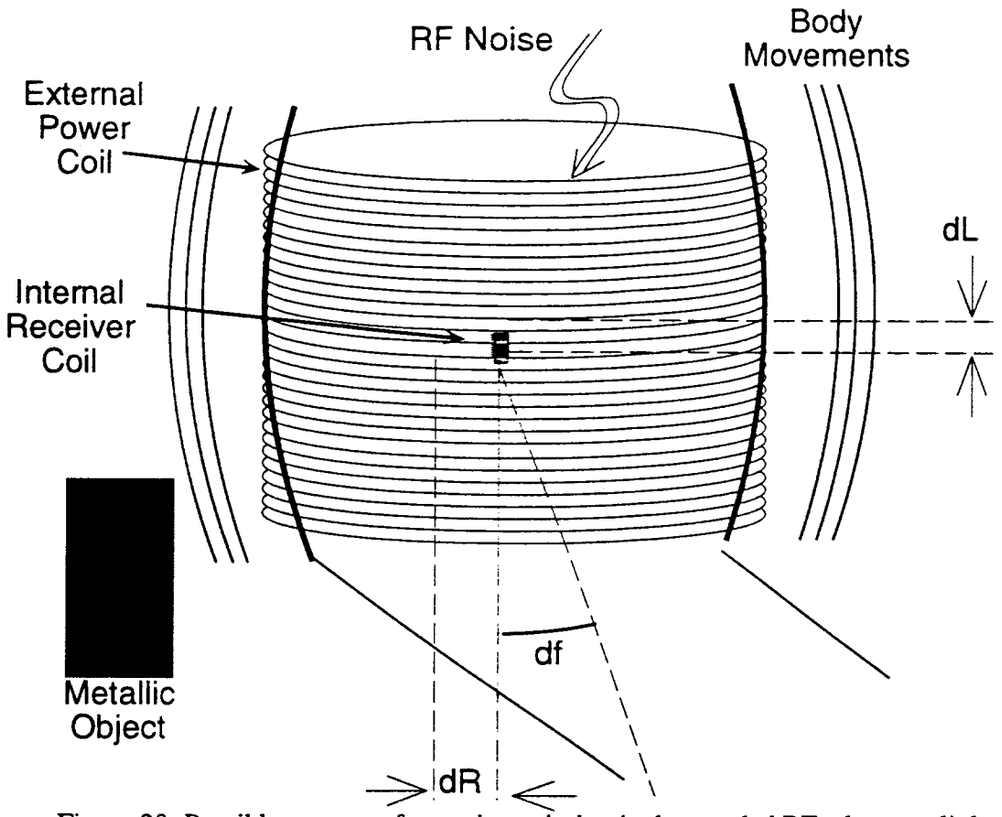

Figure 23: Possible sources of error in an inductively coupled RF telemetry link.

Any errors that do occur in data transmission will manifest themselves in one of the following ways: the envelope could fail to switch when it is supposed to; it could switch later than expected; a noise source could cause it to switch at a time when it should not, or even switch multiple times when it should not. These various errors are illustrated in Figure 24. In order to determine how often data transmission errors would occur, what the causes of the errors are, and how they manifest themselves, a test setup was constructed. This setup consists of a class E transmitter and coil tuned to 1.96MHz with a microstimulator receiver coil in the center of the transmitter coil. The transmitter coil was 3.5" diameter, 3.5" height, contained 40 turns and was 122μH with a Q of 270 measured at 1.96MHz. Using this setup, the possible sources of errors shown in Figure 23 were investigated. It should be noted that this setup is not exactly the same as the real application would be. Any sources of error that might be introduced by body tissue are not considered, since these are not felt to be of any major concern.

The first thing noted in doing these tests was that there were two forms of failure in data transmission. The first form of failure was when the microstimulator could not receive enough power and all of the on-chip circuitry would fail. In order to determine when this could happen, The microstimulator was tested in various positions inside of a coil and with several loading factors. The results of power reception are listed in Table 11, and are normalized to a case of the microstimulator receiving power in the center of an unloaded coil. Figure 25 gives the relative positions of each measurement listed in Table 11. From this table it can be seen that the worst condition for losing power to the microstimulator is if it is outside of the transmitter coil. At 1" outside of the coil, the received voltage drops to ≈40% of the center, and even at the coil edge

the voltage drops to 60% of the center. When the microstimulator is inside of the transmitter coil, the received voltage was never found to drop to less than 60% of normal due to any other condition, even a 90° misalignment of the receiver coil. Under normal operating conditions, however, power failure would likely begin to occur at any voltage drop to less than 70% of normal. If that were the case, the only conditions that would cause the microstimulator to experience power failure are misalignment of more than 60° or loading of the transmitter coil by another highly coupled coil that is tuned to the same frequency.

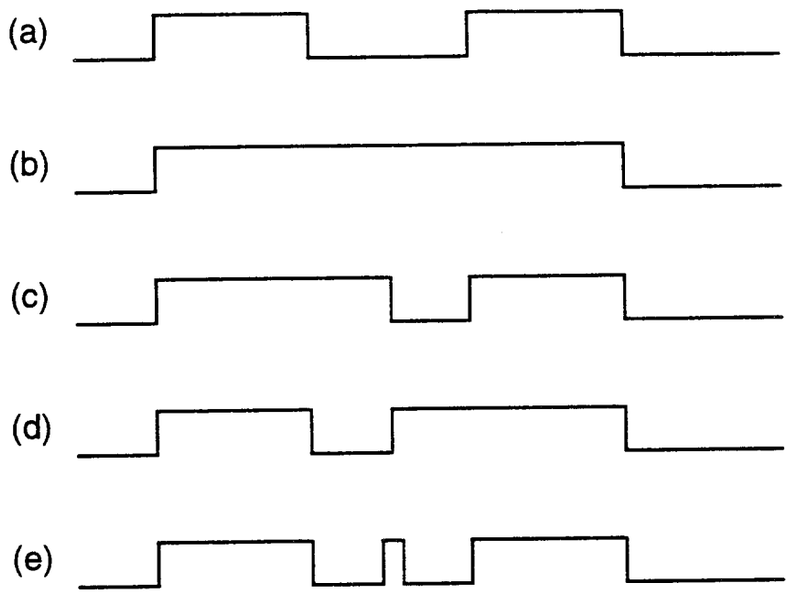

Figure 24: Manifestation of data transmission errors. (a) Expected data to be received; (b) Failure to detect transition; (c) Transition delayed; (d) Single transition at the wrong time; (e) Multiple transitions at the wrong time.

Table 11: Power reception measurements for the microstimulator.

Position of Measurement	Normalized Peak Voltage Received	Conditions of Measurement
1	1.0	No loading or misalignment
2	1.26	No loading or misalignment
3	0.63	No loading or misalignment
4	0.68	No loading or misalignment
5	0.42	No loading or misalignment
6	0.42	No loading or misalignment
1	0.84	Large iron block <1cm outside the coil, loading it
1	0.84	An identical tuned transmitter and coil is 3" away, but not turned on.
1	0.63	An identical tuned transmitter and coil is <1cm away, but not turned on.
1	0.84	No loading but receiver coil is 60° out of alignment
1	0.63	No loading but receiver coil is 90° out of alignment
1	0.95	Coil warping to an oval with major/minor axes of 1.5
1	0.84	Coil warping to an oval with major/minor axes of 2

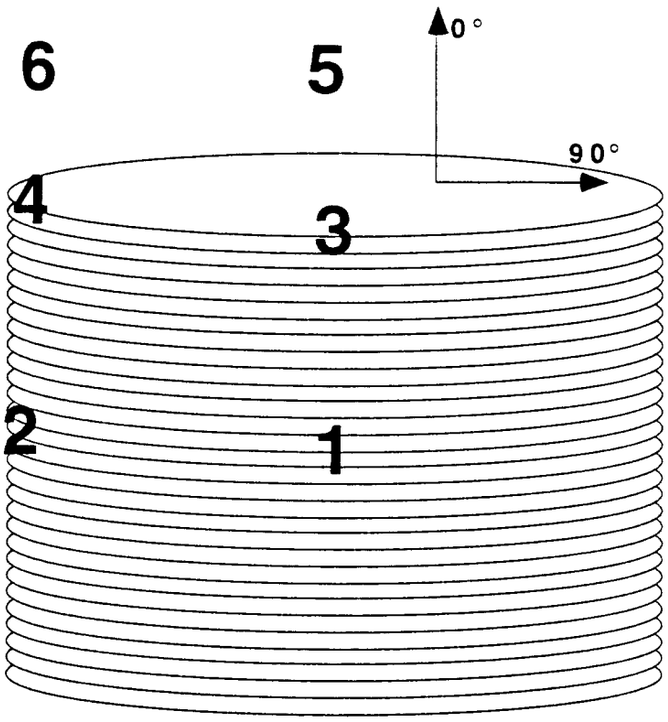

Figure 25: Positions for power reception measurements in a transmitter coil: 1) Center of coil; 2) Center of edge of coil; 3) Top center of coil; 4) Top edge of coil; 5) Center 1" above coil; 6) Edge 1" above coil.

The second form of error in data transmission is due to RF noise causing the envelope detection circuitry to switch when it should not. The microstimulator circuitry is being operated by a class E transmitter that is generating an extremely large electromagnetic field, and in trying to generate RF noise in tests, it has been observed that the only way to do this is to have another RF noise source generating comparable size field very close, such as another class E transmitter driving other microstimulators. In addition, since the microstimulator is tuned to a given carrier frequency, it was found that an external noise source will only interfere with the data transmission if it is very close to the same frequency. Table 12 lists the results of operating two class E transmitters in close proximity to each other while testing the data received by a microstimulator. It was observed that only a noise source generating a very large EM field within less than one foot of the transmitter and at a frequency <285kHz away from the carrier frequency could produce any spurious errors in data transmission.

3. ACTIVITIES PLANNED FOR THE COMING QUARTER

Work on the various aspects of the project will continue in the coming quarter. We will continue to pay close attention to our accelerated long-term soak tests in both saline and DI water, with the main focus being on the testing of the new glass capsules fabricated using ultrasonic micromachining. We hope to increase the number of samples under test and will

address the issue of silicon dissolution in more detail. We will also continue to explore other testing techniques and accelerating factors to qualify and verify our mean-time-to-failure results.

The second area of importance for us is the fabrication and assembly of prototypes of the single-channel microstimulator and its delivery to interested users. We have a number of investigators who have expressed interest in receiving and testing these devices and we are exerting our best efforts to provide the microstimulators so that we can obtain in-vivo results for the first time from these devices. We hope that by the end of the coming quarter we can address this important need and provide the devices to the external community.

Our efforts on the development of the second-generation microstimulators will also continue. Our interactions with potential users have indeed indicated that there is a great need for these multichannel devices for applications such as stimulation of the peripheral nervous system. Many of these applications do not require the bi-directional telemetry link as yet, however, they do need the multiple feedthroughs that our technology provides. We hope to be able to provide these devices also in the near future. This may require the refabrication of a new set of devices that can be used in a variety of applications. We also realize that in order to simplify the packaging and assembly of microstimulators we need to replace the hybrid components, including the capacitor and the receiver coil with their on-chip counterparts and we are carrying out studies and are exploring new technologies that can for the first time allow us to develop a fully integrated device. We will report on our findings in this area in future progress reports.

Table 12: Results of operating two class E transmitters in close proximity to each other

Ratio of operating frequencies between amplifiers (f_1/f_2)	Conditions of operation for no errors transmitted to the microstimulator
1.0	Coils must be >12" away from each other while both are being amplitude modulated
1.0	Coils must be >8" away from each other if the "noise source" amplifier is on but is not being amplitude modulated
1.16	Coils must be >2" away from each other while both are being amplitude modulated
1.16	Coils can be <1cm away from each other if the "noise source" amplifier is on but is not being amplitude modulated